JOURNAL OF CATALYSIS 98, 411–433 (1986)

Zeolite-Encapsulated Platinum Catalysts: Preparation, Characterization by Transmission Electron Microscopy, and Their Shape Selective Behavior toward Various Nitrogen Base Poisons during the Catalytic Oxidation of Aqueous Formaldehyde

TIMOTHY R. FELTHOUSE AND JUDITH A. MURPHY

Central Research Laboratories, Monsanto Company, St. Louis, Missouri 63167

Received July 30, 1985; revised November 19, 1985

Procedures are described for the encapsulation of Pt metal crystallites by the hydrogen forms of zeolite Y, mordenite, and ZSM-5. The Pt metal crystallite size and distribution in these well-encapsulated Pt/zeolite samples have been established through the use of transmission electron microscopy. Particle size ranges for the Pt crystallites are as follows: Pt/HY, 10–20 Å; Pt/H-MOR, 6–15 Å; and Pt/H-ZSM-5, 5–20 Å. Supported Pt metal crystallites effectively catalyze the oxidation of aqueous formaldehyde to carbon dioxide and water in an autoclave reactor at 95°C and 207 kPa O_2. The rate of this oxidation is extraordinarily sensitive to the presence of nitrogen bases that effectively poison the Pt sites. Nitrogen bases investigated in this study include glycine, ethylenediaminetetraacetic acid, pyridine, quinoline, and 4-methylquinoline. Reactor evaluation of well-encapsulated Pt/zeolite catalysts for formaldehyde oxidation in the presence of small amounts of these nitrogen bases demonstrates clearly that the Pt crystallites reside in regions of the zeolite structure accessible only through the crystalline zeolite pore structure. Nitrogen bases too large to penetrate the zeolite pores are found to have little or no effect on the formaldehyde oxidation rate. In the case of Pt/ZSM-5, poisoning by quinoline occurs rapidly but 4-methylquinoline shows little effect on the rate of formaldehyde oxidation even in high concentrations and for prolonged periods of exposure to the catalyst. Complete details will be given for these selective poisoning experiments with the encapsulated Pt/zeolite catalysts.

INTRODUCTION

Although molecular shape selective behavior by zeolites has been known for more than 25 years (*1, 2*), the full scope of reactions and other phenomena possible with crystalline microporous solids has yet to be realized. Incorporation of metal-containing species into the zeolite host affords extension of catalytic chemistry into the area of nonacid-catalyzed reactions (*3–9*). However, in an appreciable number of these metal–zeolite-catalyzed reactions, either the reactions studied do not involve shape selective catalysis (*10, 11*) or the catalysis mediated by the metal species is independent from effects of the zeolite. In order for the metal–zeolite catalyst to display shape selective catalysis, the metal crystallites or complexes must be encapsulated entirely within the intracrystalline space of the zeolite host.

Several novel approaches have been developed for encapsulation of metal species within the intracrystalline zeolite channels or cages. Ion-exchange techniques have been used in early work with the $Pt(NH_3)_4^{2+}$ cationic complex exchanged into NaA (*1, 2*), CaY (*12*), and hydrogen-mordenite (*13*) forms of zeolites. Recent work by Dessau (*14, 15*) has extended these exchange techniques to various forms of ZSM-5. Ion-exchange of faujasite zeolites with Fe^{2+}, Co^{2+}, or Ni^{2+} followed by introduction of the appropriate ligands have yielded metal chelate complexes that have been studied in connection with selective oxidation catalysis (*16–19*). *In situ* zeolite syntheses have trapped $Pt(NH_3)_4^{2+}$ in zeolite A (*20, 21*) and ZSM-5 (*22*) and recently various Rh

0021-9517/86 $3.00

complexes in zeolites A (*21, 23*) and Y (*24*). The strong acid sites present in the intracrystalline region of thermally treated zeolites have provided a strategy for specific deposition of organometallic complexes of Mo (*25*), Rh (*26*), Pd (*25*), and Pt (*25*) onto the interior zeolite surfaces where protonolysis of acid-labile ligands fixes these complexes within the zeolite micropores. Finally, zero-valent clusters of iron and cobalt have been deposited into the faujasite supercages using metal atom vaporization techniques to yield encapsulated metal/zeolite catalysts for Fischer–Tropsch synthesis (*27, 28*).

Among the various techniques listed above to entrap metal species within zeolite pore structures, ion-exchange methods are by far the most prevalent. Over the past 20 years numerous studies (*12, 29–44*) have appeared on the preparation and characterization of Pt crystallites in faujasite-type zeolites. Although ion-exchange with $Pt(NH_3)_4^{2+}$ invariably has been used to prepare the precursor catalyst, it is clear from the published literature that both the specific form of the faujasite and the sequence of gas-thermal treatments are critical to the attainment of zeolite-encapsulated Pt crystallites.

Various supported noble metal catalysts, particularly those containing platinum, oxidize aqueous solutions of formaldehyde to carbon dioxide quite efficiently at 95°C and 207 kPa O_2 pressure. However, the rate of this oxidation is adversely affected by the presence of small amounts of soluble nitrogen-containing bases (or other bases) that adsorb onto the Pt crystallites and block the formaldehyde oxidation reaction. One approach to circumvent catalyst poisoning is to coat a supported platinum catalyst with a permselective membrane such as polydimethylsiloxane as was recently reported in work from this laboratory (*45*). An alternative approach detailed in this work explores a variation of reactant selective catalysis (*11*) with zeolite-encapsulated Pt crystallites. In this approach small molecules such as formaldehyde, water, oxygen, and carbon dioxide diffuse rapidly through the zeolite pore structure (for pores greater than ca. 5 Å) while larger nitrogen-containing molecules that may poison the Pt sites within the zeolite are excluded from the crystalline pore structure on the basis of their molecular size.

From the prior studies of faujasite-encapsulated Pt crystallites, several parameters may affect the final Pt particle size and distribution. In this work extensive use of transmission electron microscopy (TEM) has been made to establish the precise conditions necessary to prepare well-encapsulated Pt/zeolite catalysts and to characterize in detail those samples in which the Pt crystallites reside entirely within the interior of the zeolite particles. In addition to zeolite Y, mordenite (MOR) and ZSM-5 were also examined as supports for Pt crystallites. With these well-encapsulated Pt/zeolite catalysts in hand, selective poisoning experiments were conducted during aqueous formaldehyde oxidation. Poisoning probe molecules for the encapsulated Pt catalysts include glycine (gly), ethylenediaminetetraacetic acid (H_4EDTA), pyridine (py), quinoline (quin), and 4-methylquinoline (4-Me-quin). As these liquid-phase poisoning experiments will clearly demonstrate, some remarkable selectivities are possible in terms of the nitrogen bases excluded from the encapsulated Pt crystallites.

EXPERIMENTAL

Materials. All chemicals were generally reagent grade and used as received except where otherwise noted. Formaldehyde (Fisher Scientific) was used as a 37% aqueous solution. Platinum catalyst precursor complexes included $Pt(NH_3)_4Cl_2$ (Strem Chemicals, Inc.), $Pt(NH_3)_4Cl_2 \cdot H_2O$ (Johnson Matthey), and $Pt(NH_3)_2(NO_2)_2$ (Engelhard, Lot Pt-34, aqueous solution with 4.0 g Pt/100 cm^3). Microspheroidal silica was obtained from Grace (grade 56). Chlorine-terminated polydimethylsiloxane

was purchased from Petrarch Systems (PS 375).

Zeolite samples were obtained from various commercial sources as follows: NaY (LZY52, Union Carbide), NH_4^+-exchanged NaY (LZY72, Union Carbide), NH_4Y (LZY82, Union Carbide), and NH_4-MOR (LZM8, Union Carbide). All NH_4^+ ion exchanges noted above were performed with 2.25 *M* NH_4Cl at 95°C followed by filtration and washing with water until Cl^- free. These exchanged zeolites were dried in a vacuum oven overnight at 80–100°C then sieved to below 200-mesh before further treatment. Samples of NH_4-ZSM-5 were obtained by hydrothermal synthesis at 170°C for 7 days in a Teflon-lined 300-ml Parr bomb following procedures derived from several publications (*46–48*). After washing the crystallized zeolite thoroughly, it was calcined at 540–550°C for 10–20 h. The calcined ZSM-5 samples were converted to the NH_4^+ forms by three ion exchanges with NH_4Cl solution at 25°C (*49*).

Catalyst Preparations

Zeolite-encapsulated Pt catalysts. To an aqueous stirred slurry of NH_4-zeolite (NH_4Y, NH_4-MOR, NH_4-ZSM-5) was added dropwise an aqueous solution of $Pt(NH_3)_4^{2+}$ such that the final concentration of the Pt complex was 0.019–0.029 *M*. The exchange was continued at 25°C for 12–24 h. The $Pt(NH_3)_4^{2+}/NH_4$-zeolite was rinsed free of Cl^- ion and dried overnight in a vacuum oven at 80–100°C under a dynamic vacuum (25 mm Hg) with nitrogen gas purge. The dried exchanged zeolite was crushed to below 200 mesh, mixed with 8–14 mesh silica–alumina aggregates, and packed between quartz wool plugs into an upflow dip-tube style quartz reactor. The reactor was composed of a 25-mm outer quartz tube and a 19-mm inner quartz tube. The latter tube held the catalyst-aggregate particles and was tapered to a 1/4-in. exit tube. The quartz tubes were connected to the reactor head with modified Swagelok fittings using Teflon ferrules for seals. The reactor head contained a four-way Whitey valve that allowed isolation of the treated catalyst from the atmosphere (*vide infra*).

Controlled gas and thermal treatments of the $Pt(NH_3)_2^{4+}/NH_4$-zeolite precursor catalyst were performed in an integrated facility under direct computer control. Multizone furnaces advanced to prescribed temperatures or progressed at linear thermal ramping rates under a PID algorithm. All gases (Ar, O_2, H_2) were mass flow controlled and could be blended to a range of compositions. Typically the quartz reactor containing the precursor catalyst was placed in the furnace for thermal equilibration while a purge of Ar at 10–60 cm^3/min passed through the catalyst bed. A quartz thermowell containing a thermocouple was placed at the middle of the catalyst bed. Gas-thermal treatments were loaded in advance into the computer through a set of sequencer programs. Reference to prior work on well-dispersed Pt/zeolite catalysts (*15, 32, 34, 35, 38*) in conjunction with our own electron microscopy data (*vide infra*) dictated the precise sequence of gas-thermal treatment used to prepare the zeolite-encapsulated Pt catalysts reported here. For $Pt(NH_3)_4^{2+}/NH_4Y$ the following sequence was used: Ar(320 cm^3/min)–O_2(80 cm^3/min) gas blend was passed through the catalyst bed while ramping at 2°C/min from 100 to 250°C followed by another ramp at 0.5°C/min from 250 to 600°C. With the O_2 off, the reactor was cooled to 300°C over a 3-h period with Ar purge. At 300°C, H_2 was blended into the Ar stream at 80 cm^3/min for 2 h after which the H_2 was shut off and the reactor cooled to 100°C under Ar purge. A similar treatment scheme was employed for the $Pt(NH_3)_4^{2+}/NH_4$-MOR and $Pt(NH_3)_4^{2+}/NH_4$-ZSM-5 catalyst precursor materials except that a single ramp from 100 to 350°C was executed at 0.2°C/min in an Ar–O_2 flow. Treated Pt/zeolite catalysts were removed from the quartz reactor and separated from the 8–14 mesh aggregates on a 50-mesh sieve.

Pt/SiO_2. A sample of Pt/SiO_2 was pre-

pared for comparison with the zeolite-encapsulated Pt compositions prepared above. An aqueous solution of $Pt(NH_3)_2(NO_2)_2$ was added to an appropriate amount (incipient wetness) of microspheroidal SiO_2 to give ca. 2% as Pt metal. The impregnated solid was first dried in air, then overnight in a vacuum oven at 50°C, and finally treated in the catalyst preparation facility described above. Under a purge of Ar at 113 cm^3/min, the $Pt(NH_3)_2(NO_2)_2/SiO_2$ was heated from 100 to 200°C. Then H_2 was blended into the Ar stream at 0.4%/12 min up to 10% H_2/Ar. The catalyst obtained was designated 1.79% Pt/SiO_2.

Silylation of Pt/HY. Freshly treated Pt/HY (*vide supra*) was isolated from the laboratory atmosphere using the four-way Whitey valve and removed from the furnace. The encapsulated Pt/HY (ca. 4 g) was taken into a Vacuum Atmospheres drybox (N_2 atmosphere), sieved free from the 8–14 mesh aggregates, and placed in a three-necked flask containing a stopper, a stopcock, and a septum. The flask was transferred to a glove bag and chlorine-terminated polydimethylsiloxane, Cl–PDMSi–Cl, was added in excess (ca. 10 ml, enough to wet the entire Pt/HY sample) along with a stir bar. The flask was removed from the glove bag and fitted with a water-cooled condenser that was vented through an oil bubbler. Dry toluene distilled from Na was added under Ar to the Pt/HY(–PDMSi–) sample to give a brown–black suspension. The toluene slurry was heated to reflux overnight. Moist litmus paper at the bubbler exit detected acid (HCl) in the Ar vent gas. The silylated Pt/HY was filtered in air and washed well with tetrahydrofuran and hexanes before drying at 100°C in a vacuum oven overnight. Prior to reactor evaluation of this catalyst for formaldehyde oxidation, the Pt/HY(–PDMSi–) sample was "wet" by a series of methanol–water mixtures by sonication of the slurry in an ultrasonic bath. Eventually this procedure resulted in good dispersion of the silylated catalyst in pure aqueous solutions.

Physical Measurements

Elemental analyses cited throughout this work were performed by Galbraith Laboratories, Knoxville, Tenn.

Catalyst particle sizes were determined using a Coulter Counter instrument. Surveys of zeolite particle sizes and morphology were made on a Cambridge Stereoscan 250 scanning electron microscope.

Transmission electron microscopy (TEM) data were acquired on all of the Pt catalysts reported here. Preliminary surveys of Pt/zeolite samples to judge the gas-thermal treatment effects on the Pt particle size and distribution were performed on a Hitachi H-600 100-keV TEM instrument at Monsanto. These samples were dispersed in an epoxy resin and cured then ultramicrotomed into thin sections less than 1000 Å thick using a diamond knife. The specimens were placed on a copper grid and coated with a light carbon film in a vacuum evaporator to improve the electron beam stability of the epoxy-embedded catalyst particles.

High-resolution electron microscopy of the well-encapsulated Pt/zeolite samples was performed on ultrasonically dispersed particles deposited onto holey carbon films. Bright field images were recorded using minimum electron beam exposure techniques. Intermediate-voltage electron microscopes used in this study included the following instruments: JEOL 2000FX (JEOL USA, Peabody, Mass.), Hitachi H-800 (Hitachi, Inc., Naka Works, Japan), JEOL 200CX (Arizona State University, Tempe, Ariz.), and Philips 430 (Philips Electronic Instruments, Inc., Eindhoven, The Netherlands).

Fourier-transform infrared (FTIR) spectra were recorded for various Pt/zeolite samples using a Nicolet 7199 spectrometer. Spectra were recorded on 13-mm pellets of the Pt/zeolite dispersed in KBr.

All zeolites investigated were characterized by their powder X-ray diffraction (XRD) pattern. XRD analyses were con-

ducted on finely ground (below 325 mesh) samples with a Scintag PAD II system using CuK_α radiation. X-ray patterns were acquired with a high-purity germanium detector maintained at 77 K and single-channel analyzer. The hydrothermally synthesized samples of ZSM-5 after calcination and NH_4^+-exchange were found to agree with a published XRD pattern (*50*).

Hydrogen chemisorption titrations were made on one Pt/H-MOR sample having predominantly zeolite-encapsulated Pt crystallites as determined by TEM. The titrations were performed at 25°C on an apparatus constructed in this laboratory and previously described (*51, 52*). Dehydration of the pretreated sample was conducted at 300°C in a stream of flowing Ar overnight prior to the chemisorption measurements.

Autoclave Reactor System and Evaluation Procedure

Selective poisoning experiments during the oxidation of aqueous formaldehyde were performed in an autoclave reactor system of which an overall schematic diagram appears in Fig. 1. All experiments reported here were done at a reactor temperature of 95 ± 3°C, 207 kPa O_2 pressure, 150 to 160 cm^3/min O_2 flow through the autoclave, and with an agitation rate of 1500 rpm. The oxygen flow through the reactor provided a continuous vent for the carbon dioxide product generated by the formaldehyde oxidation reaction. This CO_2/O_2 vent gas composition afforded a convenient means to monitor the conversion of the formaldehyde oxidation reaction by means of an in-line Wilks infrared (IR) process analyzer. Thus, with known CO_2/O_2 blends, the IR analyzer was calibrated such that the formaldehyde conversion was obtained as a function of time.

In a typical reaction 2.0 ml of 37% formaldehyde solution, 100 g H_2O, and 0.15 to 0.50 g of catalyst were added to the reactor. The reactor was sealed and the mixture heated under as slight positive pressure of O_2 with agitation at 800 rpm while the reactor temperature rose to 95°C. At 95°C, the agitation rate was increased to 1500 rpm, the pressure was increased to 207 kPa, and

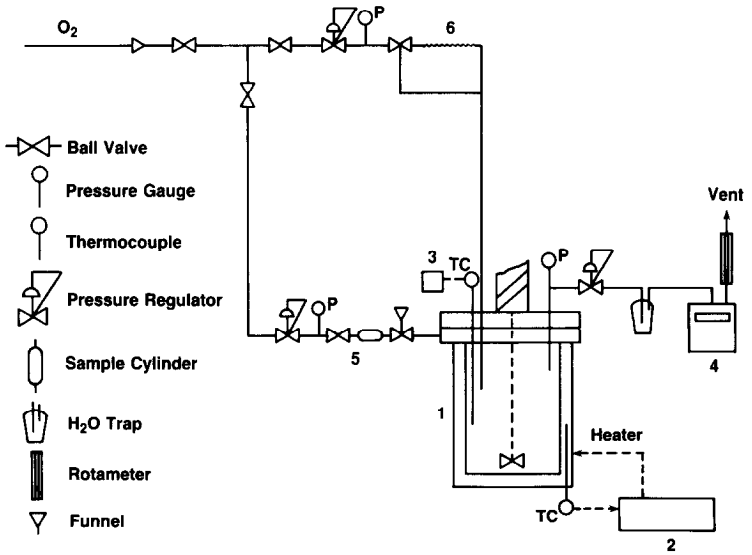

FIG. 1. Schematic diagram of stirred batch autoclave reactor system used in this work. Numbered components include: (1) Autoclave Engineers 316 stainless-steel 300-ml Magnedrive autoclave; (2) proportionating temperature controller; (3) thermocouple readout box; (4) Wilks Miran II process IR analyzer; (5) pressure cylinder assembly for formaldehyde or nitrogen base addition; and (6) O_2 bypass line for initial reactor pressurization and capillary tubing for correct flow rate during reactor operation.

the reaction was begun (time zero) with monitoring of the cumulative CO_2 recorded at approximately 3-min intervals. Prior to poisoning experiments, one or more runs were made with formaldehyde substrate (no nitrogen base present) to establish a base-level of activity for any particular catalyst. Subsequent formaldehyde charges or nitrogen bases were introduced to the reactor through a pressure cylinder entry tube in the autoclave reactor head.

RESULTS

A series of zeolite-encapsulated Pt catalysts was prepared from a $Pt(NH_3)_4^{2+}$–NH_4/zeolite precursor composition. The NH_4^+ forms were converted to hydrogen forms of the zeolites after thermal treatment. The hydrogen-zeolite forms were deemed desirable in this study since intrazeolitic diffusion would not be influenced by cations positioned within the zeolite micropore systems. Some physical properties of the Pt catalysts used in this work appear in Table 1.

The successful preparation of the zeolite-encapsulated Pt catalysts reported here requires a precise sequence of four steps. These steps include (1) ion exchange of the NH_4-zeolite with $Pt(NH_3)_4^{2+}$ to form the $Pt(NH_3)_4^{2+}$/NH_4-zeolite catalyst precursor; (2) filtration, washing, and drying of the precursor material at 80–100°C; (3) slow calcination (0.2–0.5°C/min) in flowing O_2 to 350°C (and in some instances to 600°C; see Ref. (*34*)) to 600°C; and (4) hydrogen reduction of the dehydrated-decationated zeolite at 300°C. The computer-controlled catalyst preparation facility described in the Experimental section affords investigation of several variations (e.g., no O_2 in step 3 with only Ar) of steps (3) and (4) above. However, of the alternative gas-thermal sequences used, none provided the high degree of encapsulated Pt crystallites obtained from the calcination–reduction sequence cited above.

TEM Studies

TEM examinations of the Pt/zeolite catalysts provide a direct assessment of the Pt particle sizes and distribution throughout the zeolite particles. As noted above, the precise gas-thermal treatment sequence is critical to the attainment of well-encapsulated Pt crystallites. Figure 2 depicts a representative example of the bimodal type of Pt particle size distribution when the calci-

TABLE 1

Summary of Platinum Catalysts and Their Characterization by Transmission Electron Microscopy

Catalyst	Catalyst support particle size[a] (μm)	Zeolite Si/Al[b]	TEM of Pt particles	
			Size, Å	Distribution[c]
1.79% Pt/SiO_2	74–595[d]	—	15–40	M
2.93% Pt/HY	1.47	3.6	10–19	M
3.23% Pt/HY(–PDMSi–)	1.48	9.1[e]	10–15	M
3.57% Pt/H-MOR	1.06	8.0	6–15	M
3.66% Pt/H-MOR	1.06	8.0	6–15, 30–520[f]	B
3.54% Pt/H-ZSM-5	5.54	16.9	5–20	M
3.17% Pt/H-ZSM-5	—[g]	14.4	5–20, 25–300	B

[a] Average zeolite particle size from Coulter Counter measurements.
[b] Ratios determined by elemental analyses of Pt-free NH_4^+-zeolites.
[c] Pt distribution codes: M = monomodal, B = bimodal.
[d] Particle size range reported for Grace grade 56 microspheroidal silica.
[e] From direct analysis of this Pt catalyst.
[f] Pt particles in this size range are very few.
[g] Particle size not determined but probably 5–6 μm average from prior syntheses.

FIG. 2. Transmission electron microscopy (TEM) micrograph taken at 100 keV on a Hitachi H-600 of an ultramicrotomed section of ~3% Pt/HY. When the initial calcination step is too rapid, a bimodal distribution of Pt crystallites results as seen here for the encapsulated (10–20 Å) and unencapsulated (30–200 Å) Pt particles.

nation step is too rapid. In addition to the smaller Pt crystallites of less than 20 Å, many larger Pt crystallites of 30 to 200 Å can be seen that reside on the external surface of the zeolite particles and are irregularly shaped. Striations due to imperfec-

tions in the diamond knife are visible in this ultramicrotomed sample. No direct evidence for electron beam damage was detected in this or any of the other micrographs presented here.

When the calcination step is sufficiently long to dehydrate the Y zeolite, views of the Pt/HY catalyst as seen in Fig. 3 are obtained. In view A of Fig. 3 numerous regions containing lattice fringes are observable as a result of the zeolite lattice and the electron beam being in a diffracting condition. For the cubic zeolite Y lattice, the cell constant is between 24 and 25 Å (*53, 54*) depending upon the identity of cationic species that charge balances the anionic zeolite framework. In Fig. 3A the lattice fringes show a repeat distance of ca. 24.5 Å in good agreement with the expected HY zeolite lattice cell constant. View B of Fig. 3 provides the best assessment of the Pt particle size in the HY zeolite with a range of 10 to 19 Å for these Pt particles. In contrast to the sintered Pt particles in Fig. 2, these Pt particles are relatively homogeneously distributed and spherical in shape.

Figure 4 displays well-dispersed Pt particles of some 6 to 15 Å on a H-MOR sample. Despite several attempts with different electron microscopes, no lattice fringes attributable to the H-MOR support were observed. However, close inspection of the Pt crystallites themselves on a 200-keV microscope reveals lattice fringes. Figure 5

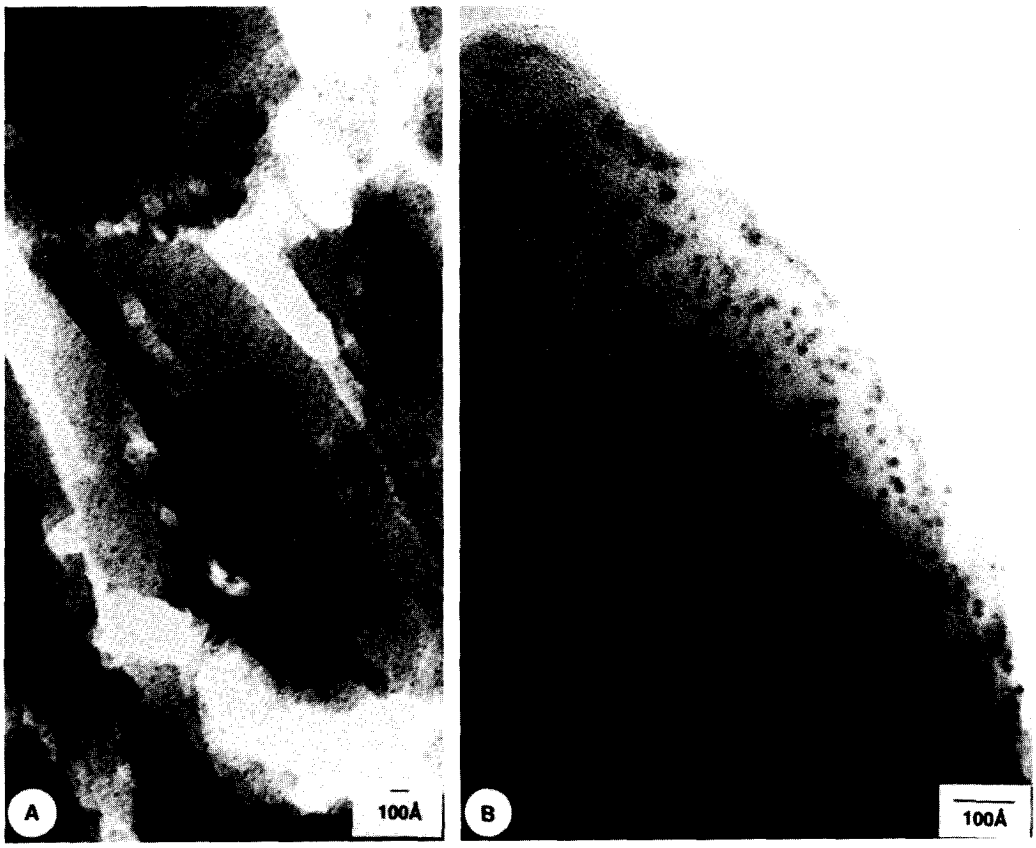

FIG. 3. Two views of well-encapsulated 2.93% Pt/HY. In view A, TEM of an ultramicrotomed section recorded at 100 keV on a Hitachi H-600 shows both Pt crystallites and the presence of lattice fringes of the Y zeolite with a repeat distance of ~24.5 Å, the unit cell length of zeolite Y. View B was taken at 200 keV on a JEOL 2000FX of a Pt/HY particle protruding over a holey carbon film with Pt crystallites of 10 to 19 Å.

FIG. 4. TEM micrograph taken at 200 keV on a Hitachi H-800 of well-encapsulated 3.57% Pt/H-MOR showing spherical-shaped Pt crystallites of 6 to 15 Å.

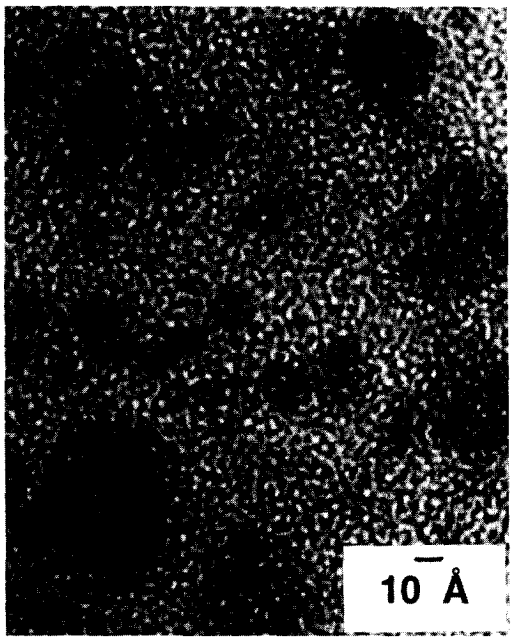

FIG. 5. Closeup of a sample of well-encapsulated 3.30% Pt/H-MOR recorded at 200 keV on a JEOL 200CX. Note the presence of lattice fringes in the Pt particle (arrow) on the MOR support.

shows the Pt particle lattice fringes of some 2.3 Å (*55*) and provides evidence that the crystallites observed in the zeolite studied here are single crystals and not twinned ones.

A well-encapsulated 3.54% Pt/H-ZSM-5 sample was subjected to TEM characterization and found to have a uniform distribution of Pt crystallites from preliminary observations of the ultramicrotomed specimens. Better definition of the small Pt crystallites is obtained on intermediate-voltage electron microscopes with representative views shown in Fig. 6. The Pt particles range from 5 to 20 Å in size and clearly reside within the H-ZSM-5 particles. With a large aperture on the TEM instrument, direct imaging of the H-ZSM-5 lattice is obtained. Figure 7 presents two structural views of H-ZSM-5 where the white dots represent the ZSM-5 channel openings and the black dots seen in the top view represent Pt particles with the contrast reduced due to the large aperture used to include the lattice information. The morphology of the Pt/H-ZSM-5 specimen in the area where the particle protrudes over a hole in the carbon film suggests that there are fringes which occur in nonoverlapping regions. This supports the assignment of these fringes as lattice fringes rather than a moiré effect. The observed lattice spacings are consistent throughout the entire sample with values equal to those reported for ZSM-5.

FTIR Spectra of Silylated Pt/HY

To improve the poisoning resistance (*vide infra*) to various nitrogen bases, well-encapsulated samples of ca. 3% Pt/HY were treated with oligomeric Cl-PDMSi-Cl under anhydrous conditions. An FTIR study was undertaken with air-exposed (i.e., rehydrated) samples of Pt/HY and Pt/HY(–PDMSi–) in order to provide evidence for the existence of the siloxane coating on the zeolite surface.

Figure 8 displays an FTIR difference spectrum from which the absorptions present in the parent Pt/HY sample were subtracted from those in the Pt/HY (–PDMSi–) sample. Assignment of the difference bands in the hydroxyl region labeled in Fig. 8 remains ambiguous due to variable degrees of hydration in the two samples. However, this difference spectrum permits distinct identification of bands attributable to PDMSi fragments now present in Pt/HY. The asymmetric —CH_3 stretch appears at 2970 cm^{-1}, the symmetric —CH_3 stretch at 2915 cm^{-1}, the asymmetric —CH_3 deformation at 1415 cm^{-1}, and the symmetric —CH_3 deformation at 1275 cm^{-1}. These vibrations closely match the analogous ones for polydimethylsiloxane polymers in both band positions and their relative intensities (*56*).

Powder XRD Data

All of the ammonium zeolite supports used in this work were relatively crystalline samples as judged from their powder XRD patterns. In the case of Pt/HY and Pt/H-

ZSM-5 obtained after controlled gas-thermal treatment of the $Pt(NH_3)_4^{2+}/NH_4$-zeolite precursor, Figs. 3 and 7 clearly show evidence of long-range crystalline order in HY and H-ZSM-5, respectively, as revealed by the lattice fringes in the TEM micrographs. For the H-MOR sample derived from NH_4-MOR (LZM8), no lattice fringes were detected in any Pt/H-MOR specimen despite numerous TEM micrographs recorded on this sample. As can be seen in Fig. 9, the powder XRD patterns show that the relative crystallinity of the H-MOR support remains closely similar in a pure calcined sample (tracing B) and a sample containing encapsulated Pt crystallites (tracing A).

Hydrogen Chemisorption Study of 3.66% Pt/H-MOR

A well-encapsulated Pt/H-MOR sample

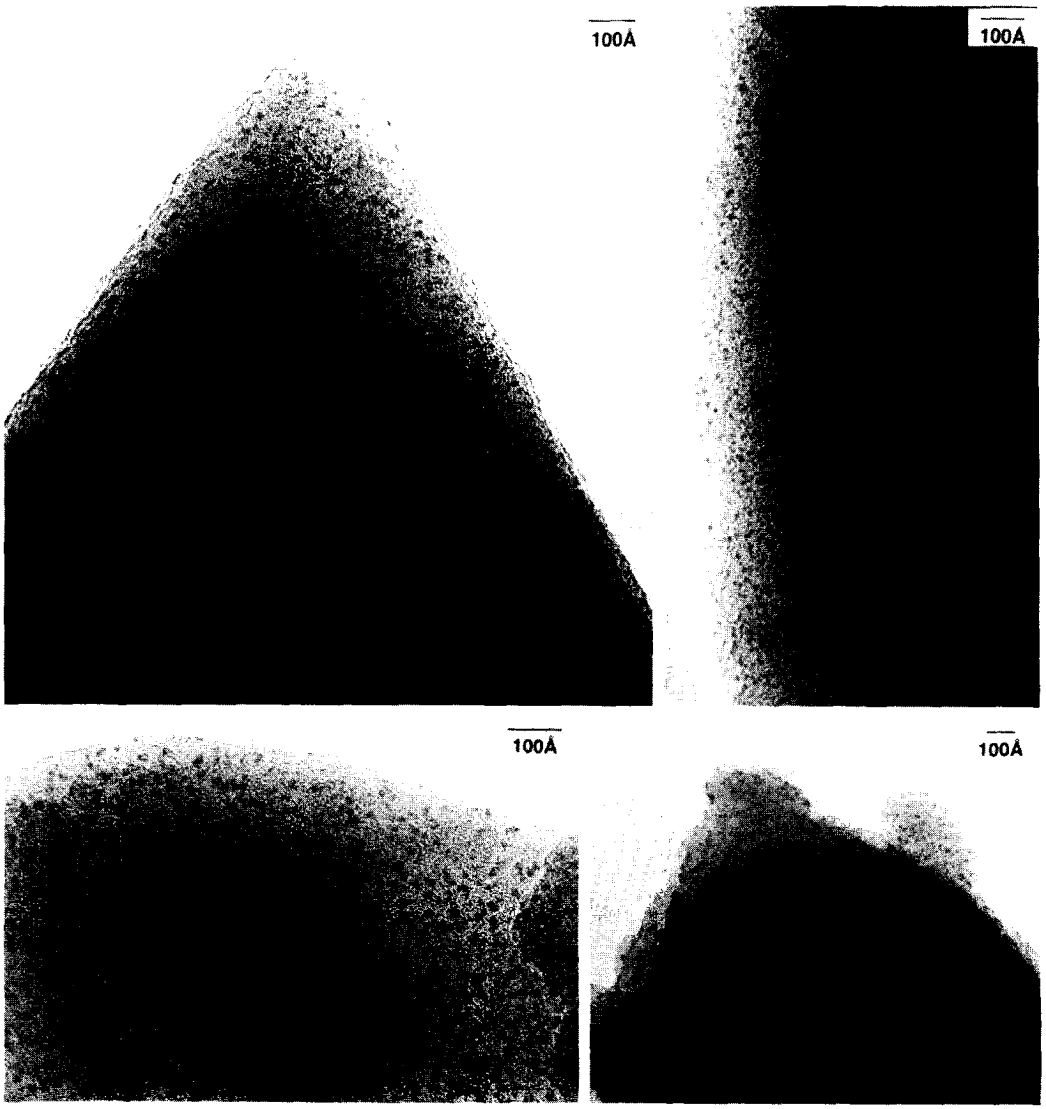

FIG. 6. TEM images of well-encapsulated 3.54% Pt/H-ZSM-5 taken with a small aperture with Pt particles in the range of 5 to 20 Å. The view in the lower right corner was recorded at 200 keV on a JEOL 2000FX; all other views were recorded at 300 keV on a Philips 430 TEM instrument.

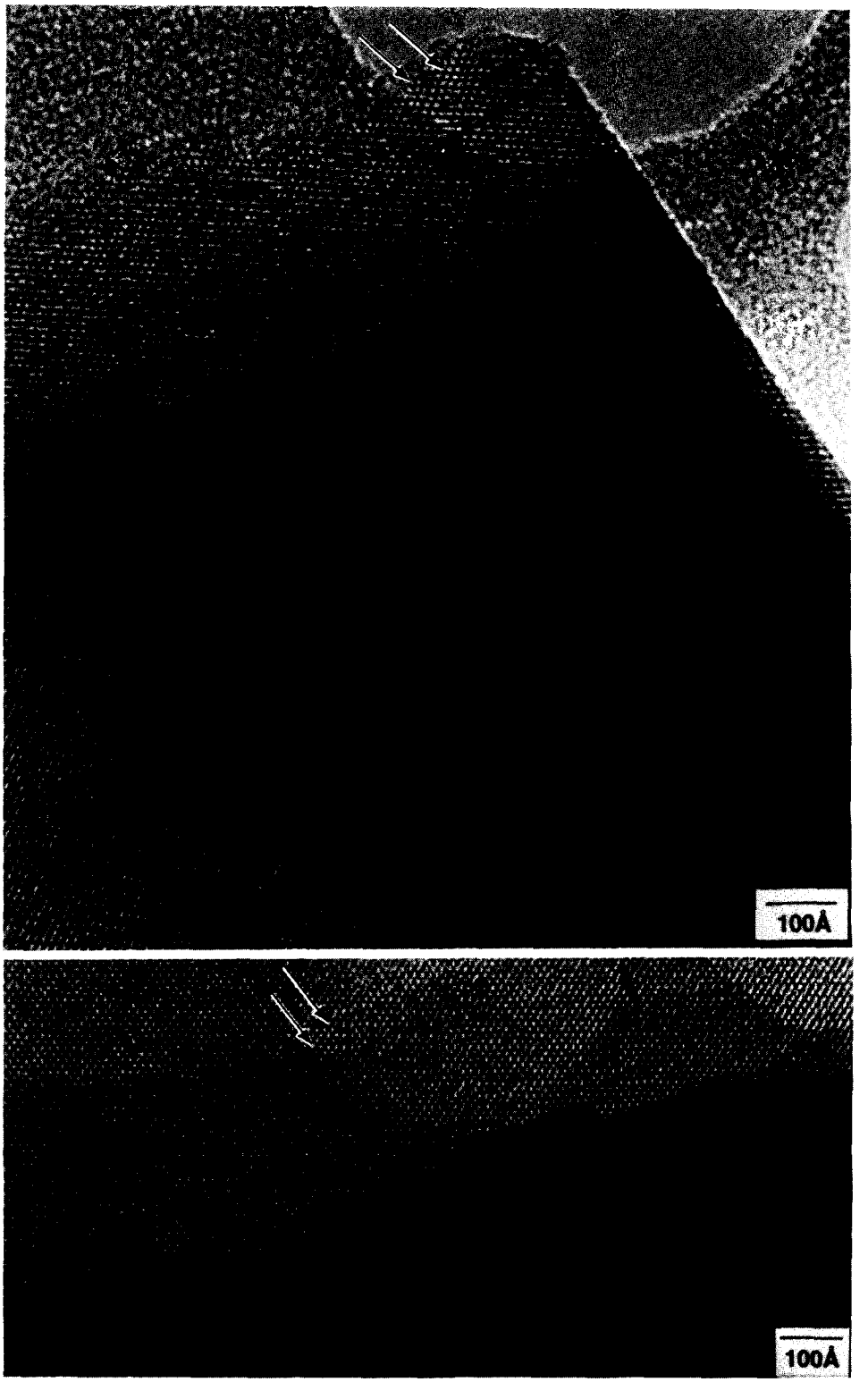

FIG. 7. Two views of 3.54% Pt/H-ZSM-5 recorded at 200 keV on a JEOL 2000FX with a large aperture that affords imaging of the ZSM-5 support. The four black and white arrows point out representative channel openings of the ZSM-5 particle while the two black arrows show Pt crystallites within the ZSM-5 particle.

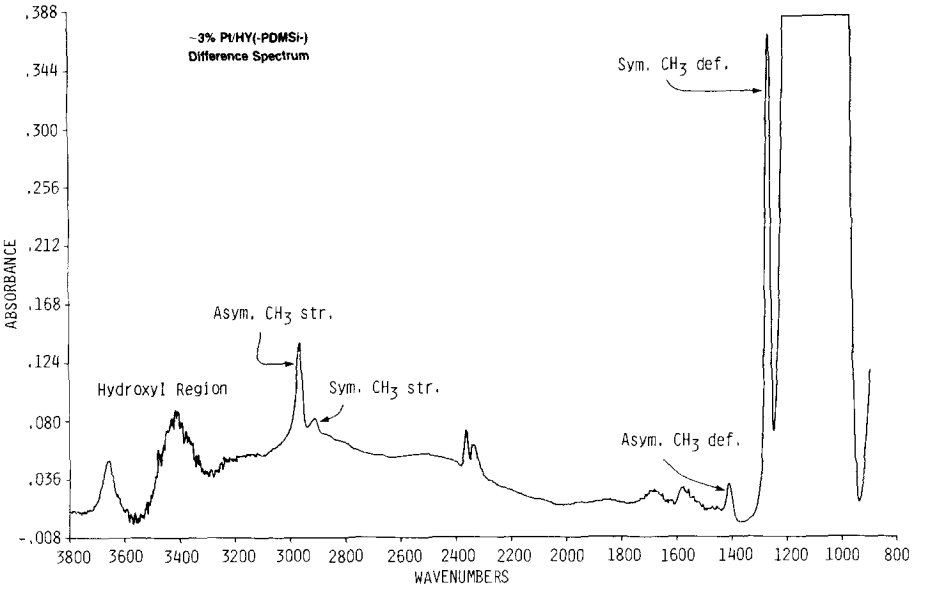

FIG. 8. FTIR difference spectrum for ~3% Pt/HY(–PDMSi–) that reveals the presence of the asymmetric and symmetric stretching and deformation bands of PDMSi. Samples used to obtain the difference spectrum were formed as KBr pellets. This spectrum was scaled to enhance the PDMSi bands present.

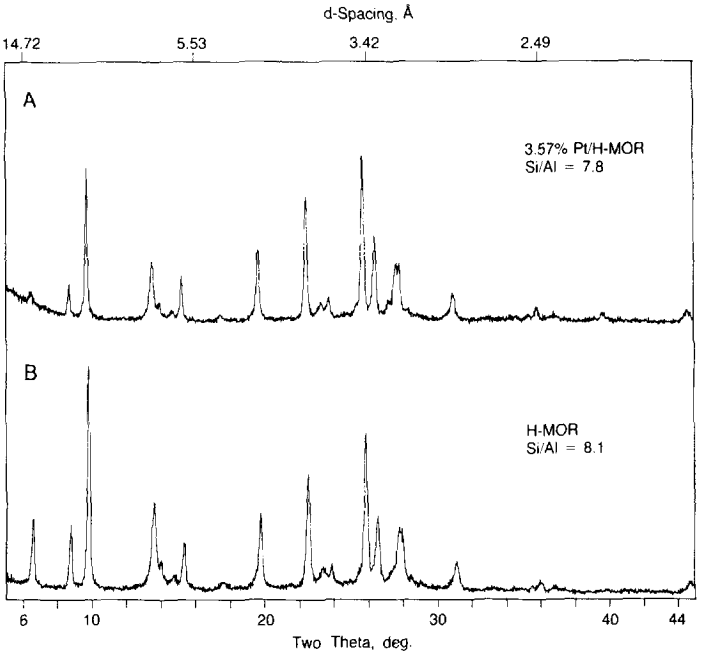

FIG. 9. Powder XRD patterns that compare the crystalline phase present in H-MOR (tracing B) after a 550°C calcination in air of NH_4-MOR and 3.57% Pt/H-MOR (tracing A) after a slow 350°C calcination in flowing O_2/Ar followed by a 300°C reduction in H_2/Ar. Tracing A confirms retention of the overall MOR structure in the catalyst after encapsulation of the Pt crystallites.

was prepared as described in the Experimental section and found to consist mostly of small Pt particles of 6 to 15 Å as summarized in Table 1. Reproducible H/Pt ratios were obtained only after this Pt/H-MOR catalyst is treated in H_2 at 25°C (after air exposure for an extended length of time) followed by overnight purging in Ar at 300°C. Chemisorption measurements were then performed at 24 to 26°C. Three independent measurements on this sample containing 187.6 μmol Pt/g catalyst produced 191.4, 188.5, and 201.8 μmol H/g catalyst with H/Pt ratios of 1.02, 1.00, and 1.08, respectively.

Formaldehyde Oxidation and Selective Poisoning Experiments

Table 2 presents a compilation of formaldehyde oxidation experiments for various catalysts with the effects of added nitrogen bases on the rate of formaldehyde oxidation. As can be seen from the molar ratios of added bases to Pt present, at all times a sufficient excess of the nitrogen base is present in the reactor to coordinate to all surface Pt atoms. In a control experiment, it can be seen that a sample of NaY zeolite has some activity for formaldehyde oxidation although this is negligible (turnover frequency, $T_N < 0.13$ mol H_2CO/h/g catalyst) compared to when a Pt-containing catalyst is present. Furthermore, once a base (e.g., H_4EDTA) is added to the reaction mixture, the activity for this "surface"-induced oxidation reaction is diminished ($T_N = 0.008$) by more than a factor of 10.

The 1.79% Pt/SiO_2 catalyst is representative of supported Pt catalysts where little or no effects of the support pore structure are present to restrict access of the nitrogen bases to the active Pt sites. Thus, while formaldehyde is rapidly oxidized with a turnover rate (T_N, now and hereafter in units of mol H_2CO/h/mol Pt) in excess of 1400, this activity declines to T_N values of 610 or less on addition of H_4EDTA, gly, py, or quin. Subsequent cycles of formaldehyde oxidation for these poisoned catalysts (not shown in Table 2) are even slower with little variation among the identities of the added bases.

The well-encapsulated 2.93% Pt/HY catalyst displayed the highest relative activity for formaldehyde oxidation of any of the Pt catalysts tested with T_N values in excess of 5000. Addition of zwitterionic H_4EDTA slowed this activity by more than a factor of 5 and the smaller molecule gly decreased the turnover rate of formaldehyde oxidation by more than a factor of 20. Clearly little discrimination is offered by the HY zeolite framework in restricting access to the Pt sites by these zwitterionic molecules.

In an effort to modify the zeolite surface adsorption sites and the pore structure, a well-encapsulated sample of Pt/HY was silylated with the oligomeric Cl–PDMSi–Cl molecules. As seen in Table 2, the 3.23% Pt/HY(–PDMSi–) catalyst is very effective in oxidation of formaldehyde in the absence of added base. These data are also displayed in Fig. 10 where a summary of these poisoning experiments with H_4EDTA can be seen. Although data points were collected at 3- and 6-min intervals from the start of the reaction, a comparison of these readings with those from known CO_2/O_2 blends revealed large deviations at these times. At the 9-min interval the IR detector reading began to show good agreement between the values for the reactor off-gas composition and the known CO_2/O_2 standard blends. Therefore, this time represented the first entry of formaldehyde conversion. The slow response of the detector perhaps may be attributed to the time necessary for the O_2 (after pressurization to 207 kPa) and CO_2 gases to equilibrate between the gas and liquid phases in the reactor and then achieve good mixing in the exit gas stream. Since the emphasis of this study was not on detailed reaction kinetics but rather to measure the relative formaldehyde oxidation activity for a number of new catalysts, it was felt that the analytical system used here was adequate to obtain this activity information even though some cat-

TABLE 2

Summary of Selective Poisoning Experiments Involving Various Nitrogen Bases during Formaldehyde Oxidation[a] by Pt/Zeolite Catalysts

Catalyst – nitrogen base[b]	Catalyst amount		Base amount		Molar ratios		Endpoint, min. (% Conversion)	T_N[c]
	g	moles Pt × 10^5	g	moles × 10^5	H_2CO/Pt	Base/Pt		
NaY(LZY52)	0.15						41(54.0)	
-H_4EDTA	0.15		0.34	118		100.0[d]	40(3.4)	
1.79% Pt/SiO_2	0.25	2.3			1070		45(100)	1400
-H_4EDTA	0.25	2.3	0.05	17	1070	7.4	60(57.5)	610
-gly	0.25	2.3	0.026	35	1070	15.2	60(5.2)	56
-py	0.25	2.3	0.027	34	1070	14.8	39(6.7)	110
-quin	0.25	2.3	0.044	34	1070	14.8	60(16.7)	180
2.93% Pt/HY	0.10	1.5			1640		14(100)	7000
-H_4EDTA	0.10	1.5	0.10	34	1640	22.7	39(100)	2500
							60(52.8)	870
-gly	0.10	1.5	0.026	35	1640	23.3	60(15.4)	250
3.23% Pt/HY(–PDMSi–)	0.10	1.9			1300		14(100)	5500
-H_4EDTA	0.10	1.9	0.10	34	1300	17.9	14(100)[e]	5500
							16(100)[f]	4900
							27(99.6)	2900
							60(64.4)	830
-gly	0.10	1.9	0.026	35	1300	18.4	60(17.9)	230
3.57% Pt/H-MOR	0.25	4.6			530		21(100)	1500
-H_4EDTA	0.25	4.6	0.10	34	530	7.4	20(100)	1600
							20(100)	1600
							20(100)	1600
-gly	0.25	4.6	0.026	35	530	7.6	60(55.5)	300
-py	0.25	4.6	0.031	39	530	8.5	60(89.2)	480
							60(74.2)	400
-quin	0.25	4.6	0.044	34	530	7.4	23(100)	1400
							24(100)	1300
							23(100)	1400
							21(100)	1500
3.54% Pt/H-ZSM-5	0.50	9.1			270		20(100)	810
							16(100)	1000
							15(100)	1100
-H_4EDTA	0.50	9.1	0.10	34	270	3.7	17(100)	950
							18(100)	900
							18(100)	900
							19(100)	850
-gly	0.50	9.1	0.026	35	270	3.8	60(75.1)	200
							60(78.8)	210
-py	0.50	9.1	0.027	34	270	3.7	60(20.3)	55
-quin	0.50	9.1	0.044	34	270	3.7	60(40.9)	110
-4-Me-quin	0.50	9.1	0.049	34	270	3.7	17(100)	950
							17(100)	950
							17(100)	950
							17(100)	950
3.17% Pt/H-ZSM-5	0.25	4.1			600		15(100)[g]	2400
							17(100)	2100
-4-Me-quin	0.25	4.1	0.049	34	600	8.3	24(100)	1500
							22(100)	1600
							21(100)	1700
-4-Me-quin	0.25	4.1	0.098	68	600	16.6	27(100)	1300
							25(100)	1400
-4-Me-quin	0.25	4.1	0.49	340	600	82.9	44(100)	820
							44(100)	820
							52(100)[h]	690
							52(100)	690

[a] All experiments were conducted under identical conditions with 2.0 ml of 37% formaldehyde solution (0.0246 mol H_2CO charge) and 100 g of water added to the autoclave. For details, see Experimental section.

[b] Bases added to fresh amounts of catalyst after initial H_2CO oxidation activity was established.

[c] Turnover frequency = mol H_2CO/h/mol Pt assuming all Pt is present as surface atoms.

[d] Molar ratio of H_4EDTA-to-NaY zeolite.

[e] Data for this run-series are displayed in Fig. 10.

[f] Here and in succeeding run-series, these entries represent subsequent H_2CO oxidation cycles with a fresh H_2CO charge.

[g] Data for this run-series are displayed in Fig. 11.

[h] Endpoint obtained after 18-h contact of catalyst and base upon addition of a fresh H_2CO charge.

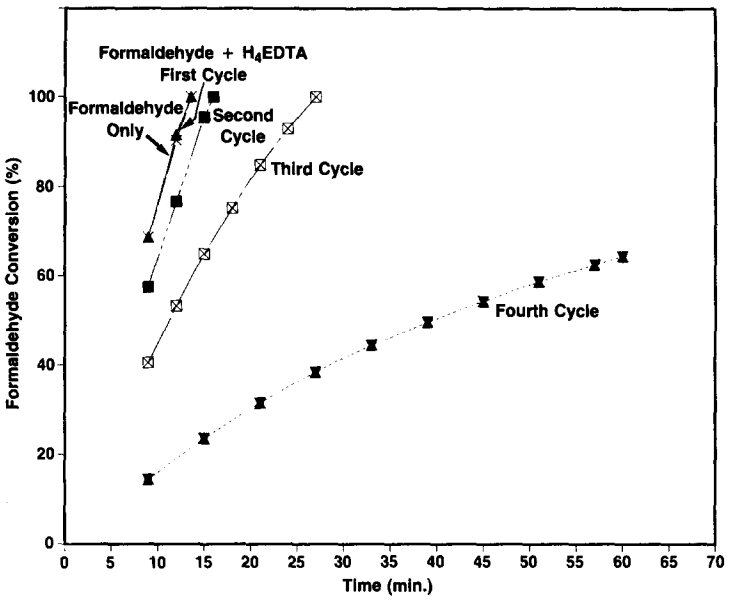

FIG. 10. Plot of the effect of H_4EDTA on formaldehyde conversion as a function of time for a sample of 3.23% Pt/HY(–PDMSi–).

alysts such as 3.23% Pt/HY(–PDMSi–) showed high levels of conversion by the time of the 9-min reading. After addition of H_4EDTA and another charge of formaldehyde to the reaction mixture, the catalyst shows essentially the same activity for formaldehyde oxidation. Subsequent cycles of formaldehyde oxidation show a steady decline in activity as the relatively large H_4EDTA molecules gradually poison more Pt sites. However, the activity of this catalyst after four cycles of formaldehyde oxidation is practically the same as the uncoated 2.93% Pt/HY catalyst after the first contact with H_4EDTA. A smaller molecule like gly, however, rapidly penetrates through the silylated coating on Pt/HY and is as effective a poison for 3.23% Pt/HY (–PDMSi–) as for 2.93% Pt/HY (compare T_N values of 230 and 250, respectively).

In order to achieve a greater degree of discrimination toward poison molecules, the smaller pore mordenite zeolite was investigated with Pt crystallites dispersed throughout the microporous channels. As reflected in the data in Table 2, the H_4EDTA molecule now is seen to have no effect on the rate of formaldehyde oxidation. The turnover frequency remains the same before H_4EDTA was added and for at least three cycles of formaldehyde oxidation after its introduction into the reactor. Smaller molecules like gly and py are seen to poison this 3.57% Pt/H-MOR catalyst almost immediately with a decline in turnover frequency for the catalyst by a factor of 3 after addition of these nitrogen bases to the reactor. However, a larger uncharged molecule like quin apparently can no longer penetrate the H-MOR pore structure since four cycles of formaldehyde oxidation with Pt/H-MOR in the presence of quin show no effect on the T_N value.

With the above selectivities demonstrated toward exclusion of H_4EDTA and quin, a Pt catalyst was evaluated in which the crystallites were observed to be within the pore structure of H-ZSM-5 by TEM (Fig. 6). Again the introduction of a large molecule like H_4EDTA shows no effect on the rate of formaldehyde oxidation by a 3.54% Pt/H-ZSM-5 catalyst. Turnover frequencies for formaldehyde oxidation range from 810 to 1100 both before and after addi-

tion of H_4EDTA. The smaller molecules gly and py both penetrate the ZSM-5 pore structure and poison most Pt sites for formaldehyde oxidation as evidenced by a reduction of the T_N values below 210. Somewhat surprisingly, the introduction of quin to the reactor results in a rapid decline in the formaldehyde oxidation rate within the first cycle of oxidation. However, an equally surprising result comes from the evaluation of the 3.54% Pt/H-ZSM-5 catalyst after 4-Me-quin is introduced into the reactor. As seen in Table 2, the catalyst now maintains a turnover frequency of 950 for four cycles in the presence of 4-Me-quin.

The above result with 4-Me-quin prompted a more extended evaluation of the effect of 4-Me-quin on the Pt/H-ZSM-5 catalyst. These results are compiled in Table 2 and also plotted in Fig. 11. From TEM data (Table 1) it is known that a few regions of this catalyst contain Pt crystallites on the external zeolite surface. Addition of 4-Me-quin shows a small decline in the turnover frequency to 1500. Now upon addition of another charge of formaldehyde, the 4-Me-quin concentration was doubled. A small reduction in the catalyst turnover frequency to 1300 is observed but the catalyst is still very effective for formaldehyde oxidation. After one additional cycle, the 4-Me-quin concentration is increased to 10 times the original value. This lowered the formaldehyde oxidation rate slightly and the Pt/H-ZSM-5 catalyst now shows a turnover rate of 800. Continued contact of the catalyst with an 80-fold excess of 4-Me-quin for 24 h results in another decline in the T_N value to 690 but this value appears to be maintained upon introduction of additional charges of formaldehyde.

DISCUSSION

In accord with previous studies of Pt/HY (*32*, *34*, *38*) and Pt/H-ZSM-5 (*14*, *15*), the preparation of highly dispersed zeolite-encapsulated Pt crystallites requires a sequence of ion exchange with $Pt(NH_3)_4^{2+}$, slow calcination in an oxygen-containing

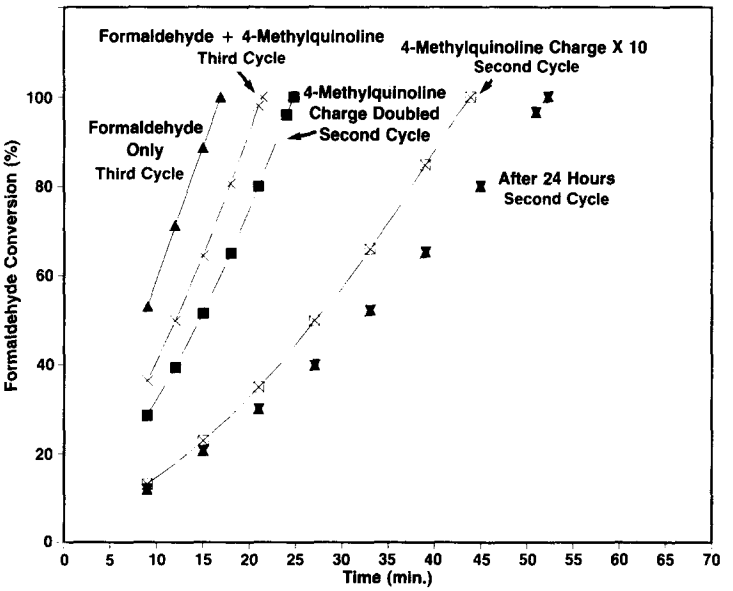

FIG. 11. Plot of the effect of 4-methylquinoline on the formaldehyde oxidation rate for various amounts of added nitrogen base. Note that even after contacting 3.17% Pt/H-ZSM-5 for 24 h, the Pt sites are still active for formaldehyde oxidation in marked contrast to the case where quinoline is present and severe poisoning occurs in the first cycle.

gas stream, and reduction in hydrogen. As seen from the TEM micrographs presented here, this procedure produces well-encapsulated Pt/zeolite catalysts from the NH_4^+ forms of zeolite Y, mordenite, and ZSM-5. The TEM image of 2.93% Pt/HY shown in Fig. 3B agrees well with previous reports (*35, 38*) that used a similar pretreatment scheme to generate the encapsulated Pt/HY. TEM images presented here for Pt/H-MOR and Pt/H-ZSM-5 appear to be among the first published micrographs of well-encapsulated Pt contained in these smaller pore zeolites.

The TEM data on the Pt/zeolite catalysts provide a definitive assessment of the Pt particle sizes which in all three zeolites span a small range (e.g., 5 to 20 Å) of diameters. In each case the smallest Pt particle sizes detected in Pt/HY (10 Å), Pt/H-MOR (6 Å), and Pt/H-ZSM-5 (5 Å) can be accommodated by the corresponding zeolite cage or channel dimensions. However, the majority of the Pt particle sizes exceeds the zeolite micropore dimensions regardless of whether the zeolite is HY, H-MOR, or H-ZSM-5. Previous studies of the calcination step in $Pt(NH_3)_4^{2+}/NH_4Y$ (*57*) have found that relatively high Pt content in conjunction with a dry oxygen-containing gas contribute to zeolite framework damage or even collapse at low (450°C) temperatures. Recent work by Schulz-Ekloff *et al.* (*58, 59*) has found that Ni-, Pd-, and Pt-containing faujasites often contain metal crystallites that far exceed the zeolite channel size. These metal crystallites are suggested to grow at the expense of the local zeolite lattice and are controlled in size by the rate of the dealumination process and the zeolite Si/Al ratio (*58*).

Formation of the larger Pt crystallites (ca. 20 Å) within the micropores of zeolite Y, MOR, and ZSM-5 that were studied here appears consistent with a dealumination process similar to that described above. Localized voids are created at the expense of the zeolite framework during the calcination and reduction treatments. The growth of Pt crystallites within these regions may occur by means of a mobile "PtH_2" species in which the zeolite pore sizes do not present impediments to migration. Such a mobile species was proposed several years ago by Dalla Betta and Boudart (*32*) to explain Pt crystallites in excess of the 7 Å pore size located within the supercages of various Y zeolites. For the HY and H-ZSM-5 zeolites containing Pt particles, Figs. 3A and 7 show clearly the zeolite lattice fringes indicative of long range order consisting of many unit cells in length. Thus, no overall structural collapse has occurred. The selective poisoning experiments demonstrate clearly with nitrogen bases that access to the encapsulated Pt sites is limited to those molecules of the appropriate size to penetrate the zeolite pores. As will be seen in more detail below, the expected kinetic diameter of the zeolite pores is generally in line with that of the nitrogen bases that can penetrate the zeolite pore structure.

A recent preliminary high-resolution TEM study of 1.8% Pt/H-ZSM-5 (*60*) concludes that the Pt crystallites in this sample reside on the external surface of ZSM-5 and not within the microporous channel regions. Evidence cited for this conclusion comes not only from comparison of the observed Pt particle size (averaging 43 Å and ranging from 15 to 90 Å) with the ZSM-5 channel size (ca. 5.5 Å) but also from a lack of distortion of the ZSM-5 lattice planes imaged about a single Pt particle. In this 1.8% Pt/H-ZSM- sample only 6% of the Pt particles is below 20 Å in diameter. In contrast, the high-resolution micrographs shown in Fig. 6 here have essentially 100% of the Pt particles below 20 Å. This 3.54% Pt/H-ZSM-5 sample lacks the broad range of Pt crystallite sizes seen in the 1.8% Pt/H-ZSM-5 material (*60*) but more importantly behaves toward potential poisons during formaldehyde oxidation in a shape selective fashion (*vide infra*). Thus, the Pt crystallites below 20 Å in the Pt/H-ZSM-5 samples investigated here are not located on exter-

nal zeolite surfaces that are easily poisoned by relatively large nitrogen bases such as H_4EDTA. However, the details of the Pt particle growth mechanism, the role of the zeolite played in the nucleation process, and the precise environment (e.g., Pt–support interactions) of the well-encapsulated Pt crystallites remain areas for further study.

One method to modify the sorption behavior of large pore zeolites such as zeolite Y is to employ organosilanes to alter the external and internal Brønsted acid sites and the pore sizes. Recent work has used hexamethyldisiloxane to modify zeolite Y for dewaxing applications (*61*), phenylmethylsilicone to treat ZSM-5 for improved *para*-alkylation of substituted benzenes (*62*), and $Si(OMe)_4$ to alter mordenite pore sizes for selective paraffin cracking reactions (*63*). Previous work from this laboratory (*45*) has found that high molecular weight trimethylsilyl-terminated polydimethylsiloxane (PDMSi) polymers are effective coatings for Pt/C catalysts for formaldehyde oxidation. These PDMSi-coated catalyst particles rapidly transport nonionic species such as formaldehyde, water, and oxygen while rejecting ionic species such as H_4EDTA. With these findings in mind, a chlorine-terminated PDMSi oligomer was tested for surface attachment to Pt/HY. The $ClSi(CH_3)_2—O—(Si(CH_3)_2—O—)_n—Si(CH_3)_2Cl$ composition where n = 3–6 with molecular weights of 425 to 600 gives oligomeric chains of at most 12 to 21 Å in length. Such chain lengths provide only small surface modifications; the PDMSi units are too short to crosslink the zeolite particles which are at least 1000 Å in diameter. FTIR data presented above clearly show the presence of these PDMSi units. As seen in the poisoning experiments of Pt/HY(–PDMSi–) with H_4EDTA in Table 2, the functionalized zeolite excludes H_4EDTA from the Pt sites for several hours during formaldehyde oxidation before poisoning of the Pt sites becomes prevalent. Further efforts to improve the PDMSi surface functionalization of Pt/HY were not pursued in light of the results obtained for the smaller pore Pt/H-MOR and Pt/H-ZSM-5 catalysts (*vide infra*) that exhibit shape selective behavior toward certain nitrogen bases. However, surface silylation techniques remain a viable alternative to smaller pore zeolites to achieve shape selectivity (*61*).

Surface science results (*64–66*) suggest that formaldehyde oxidation by platinum proceeds in a stepwise manner that parallels carbon monoxide oxidation by means of the common intermediate, adsorbed CO (*66*). Equations (1)–(3) below depict this stepwise process comprised of formaldehyde adsorption and decomposition (Eq. (1)), dissociative chemisorption by molecular oxygen (Eq. (2)), and oxidation of the adsorbed H and CO species by spectator O on Pt (Eq. (3)).

$$H_2CO \rightarrow 2H(Pt) + OC(Pt) \quad (1)$$

$$O_2 \rightarrow 2O(Pt) \quad (2)$$

$$2H(Pt) + O(Pt) \rightarrow H_2O_{(l)} \quad (3a)$$

$$OC(Pt) + O(Pt) \rightarrow CO_{2(g)} \quad (3b)$$

The overall reaction over Pt leading to the principal products in this liquid phase formaldehyde oxidation with oxygen is shown as follows

$$H_2CO + O_2 \rightarrow H_2O_{(l)} + CO_{2(g)} \quad (4)$$

In the high-vacuum experiments where oxygen coverage over Pt is controlled, Eq. (3a) reverts to a recombination of adsorbed H to yield $H_{2(g)}$ and another complex set of new thermally dependent reaction intermediates is formed. A discussion of these reactions over a clean Pt surface is given by Abbas and Madix (*65*). Furthermore, extrapolation of surface science results to the liquid-phase formaldehyde oxidation requires consideration of the state of aqueous formaldehyde. In particular, aqueous formaldehyde exists as a hydrated species, dihydroxymethylene, or in oligomeric forms of polyoxymethylene glycol (*67*)). By anal-

ogy to the general dehydrogenation mechanism by which Pt-catalyzed oxidations proceed (*68*), the anhydrous monomeric form of formaldehyde can be considered as the adsorbing species for oxidation. McCabe and McCready (*66*) studied the kinetics of gas-phase formaldehyde oxidation over Pt wire and concluded that the reaction shows a positive-order dependence on O_2 concentration and a slight negative-order dependence on formaldehyde. However, it is not known if this kinetic behavior applies to the liquid-phase oxidations studied here with supported Pt crystallites. The intent of this investigation was not to extract kinetic behavior for the formaldehyde oxidation reaction and the reaction conditions used here may not be appropriate for obtaining the intrinsic kinetic behavior of the reaction.

The principal objective of this work is to demonstrate shape selective substrate catalysis by well-encapsulated Pt/zeolites. Evidence provided towards this goal comes from the reaction endpoints or turnover numbers tabulated in Table 2. Thus, the effect of the nitrogen base poisons provides the predominant contribution to the T_N values. Several secondary parameters influence the magnitude of T_N and would require a more detailed investigation in order to assess properly their relative contributions to T_N. These parameters include N, the number of Pt atoms that constitute a catalytic site for formaldehyde oxidation; diffusivities for the various substrates (e.g., H_2CO, O_2, H_2O) and the nitrogen bases; and the Pt particle sintering rate which subtracts from the initial value of N. From the hydrogen chemisorption study of Pt/H-MOR, Pt crystallites of less than 20 Å in diameter have essentially all Pt atoms exposed to the surface. X-Ray scattering experiments (*37, 69*) on small supported Pt crystallites under oxygen show that the bulk metal structure is completely disrupted perhaps to crystallites of Pt_3O_4 (*69*). The absolute value of T_N must be attenuated by a factor that accounts for the number of reduced and oxidized Pt surface sites present in the working catalyst. For Pt catalysts (e.g., 1.79% Pt/SiO_2) with less than a dispersion of unity, the presence of bulk metal atoms further reduces the value of T_N. Mass transport effects also influence T_N and differences in zeolite particle sizes (Table 1) as well as the micropore diameters may contribute to the T_N values. Considerable variations in T_N for formaldehyde oxidation are observed with values of 5500 (Pt/HY), 1500 (Pt/H-MOR), and 770-2000 (Pt/H-ZSM-5). A range of T_N values for Pt/H-ZSM-5 occurs in different samples with the higher value (2000) found for the sample (3.17% Pt/H-ZSM-5) known to contain some large Pt crystallites on the external surface. These Pt sites are presumably more accessible to substrates and hence, a slightly higher T_N value is found. As noted earlier, the exact geometry of the Pt crystallite environment in the well-encapsulated Pt/zeolite catalysts is not known. Although all Pt atoms appear accessible to gaseous adsorbates such as H_2 from the chemisorption study of 3.66% Pt/H-MOR, the number of active sites accessible to substrates in the liquid phase may be less and perhaps not the same for each of the zeolites examined here. Questions remain as to the pore structure modifications caused by the Pt crystallites and how diffusion of both substrates (formaldehyde in water and dissolved O_2) and products (CO_2, dissolved or formed into bubbles) is affected in these catalysts. Finally, effects of catalyst sintering must be considered after prolonged operation. The well-encapsulated Pt/zeolite catalysts reported here maintain resistance to poisoning (e.g., significant formaldehyde oxidation rates) for up to periods of 1 week in duration. Therefore, effects of Pt particle sintering under these reaction conditions do not make a significant contribution to the Pt/zeolite T_N values reported here.

Selective poisoning experiments during formaldehyde oxidation with the well-encapsulated Pt/H-MOR and Pt/H-ZSM-5 demonstrate shape selective behavior toward large zwitterionic molecules (e.g.,

H_4EDTA) and bicyclic nitrogen heterocycles. Smaller molecules like gly and py rapidly poison these catalysts. In an anomalous result, the quin molecule does not poison the 3.57% Pt/H-MOR catalyst during formaldehyde oxidation despite the apparent accessibility (compared to Pt/H-ZSM-5 which does poison) of quin to the H-MOR pore structure. This result suggests that perhaps some modification of the regular H-MOR pore structure has occurred affecting transport to the catalytically active Pt sites. Perhaps the most remarkable degree of molecular discrimination toward these poison molecules comes from the Pt/H-ZSM-5 experiments. Pentasil zeolites such as ZSM-5 have offered some unique selectivities toward substituted aromatic molecules in vapor-phase hydrocarbon conversions (*70*). Experiments presented here show that quin rapidly poisons Pt/H-ZSM-5 within 60 min under formaldehyde oxidation reaction conditions (95°C). However, when the 4-methyl-substituted derivative of quin is employed in poisoning experiments, little poisoning of the Pt/H-ZSM-5 does occur even after 24 h of exposure.

The above discrimination between quin and 4-Me-quin toward Pt/H-ZSM-5 illustrates a reactant selectivity that finds direct correspondence in gas-phase experiments with these bases. Studies of quin interacting with H-ZSM-5 (*71–73*) show that quin interacts not only with external hydroxyl groups but also with hydroxyls at the pore mouths. Slow diffusion of quin into the channels of ZSM-5 has also been inferred (*73*) in acid-catalyzed inhibition experiments in the vapor phase. These observations are in complete accord with the effect of quin on Pt/H-ZSM-5 in our batch experiments at 95°C. Additionally, sorption (*74*), acid-catalyzed inhibition (*74–77*), infrared (*78*) and molecular graphics (*79*) experiments find 4-Me-quin unable to penetrate the ZSM-5 channels. In agreement with these experiments, well-encapsulated Pt/H-ZSM-5 effectively oxidizes formaldehyde in the presence of 4-Me-quin although a slight concentration dependence is observed.

CONCLUSIONS

(1) Zeolite-encapsulated Pt crystallites require a precise sequence of treatments for successful preparations.

(2) All well-encapsulated Pt/zeolites prepared here show Pt particle sizes that exceed known zeolite pore structures. Some destruction of the local pore structure is suggested but the overall zeolite particle crystallinity is maintained. Further studies of this phenomenon are needed.

(3) Pt/HY displays little resistance to poisoning by nitrogen bases during formaldehyde oxidation even after some surface silylation. Bulkier silylation reagents appear to offer opportunities for enhanced selectivity.

(4) Pt/H-MOR and Pt/H-ZSM-5 display shape selective behavior toward large nitrogen-containing poisons during formaldehyde oxidation. Pt/H-ZSM-5 shows a remarkable discrimination between quin and 4-Me-quin that is in line with adsorption behavior of these bases toward ZSM-5 in the vapor phase.

(5) TEM data in conjunction with reactor data (cf., Ref. (*15*) for a gas-phase test) provide the best means to evaluate well-encapsulated Pt/zeolite catalysts.

ACKNOWLEDGMENTS

The excellent technical assistance by G. M. Wagner and N. L. Leimgruber was greatly appreciated. The authors acknowledge G. E. Barker and F. S. Delk II for their contributions to the design and construction of the automated catalyst preparation-gas chemisorption facility. We are grateful to C. L. Schosser for providing the chemisorption measurements reported here. JEOL, Philips, Hitachi, and the Arizona State University Center for High Resolution Electron Microscopy are gratefully acknowledged for instrumentation use and staff assistance. We thank J. J. Freeman and R. L. Fischer, Jr., for acquiring the FTIR data and F. L. May for powder XRD data. Finally, P. L. Mills is acknowledged for helpful discussions on factors contributing to the kinetics of formaldehyde oxidation.

REFERENCES

1. Weisz, P. B., and Frilette, V. J., *J. Phys. Chem.* **64,** 382 (1960).
2. Weisz, P. B., Frilette, V. J., Maatman, R. W., and Mower, E. B., *J. Catal.* **1,** 307 (1962).
3. Minachev, Kh. M., and Isakov, Ya. I., *in* "Zeolite Chemistry and Catalysis" (J. A. Rabo, Ed.), ACS Monogr. No. 171, pp. 552–611. Amer. Chem. Soc., Washington, D.C., 1976.
4. Jacobs, P. A., "Carboniogenic Activity of Zeolites," pp. 183–227. Elsevier, Amsterdam, 1977.
5. Uytterhoeven, J. B., *Acta Phys. Chem.* **24,** 53 (1978).
6. Gallezot, P., *Catal. Rev. Sci. Eng.* **20,** 121 (1979).
7. Maxwell, I. E., *in* "Advances in Catalysis" (D. D. Eley, H. Pines, and P. B. Weisz, Eds.), Vol. 31, pp. 1–76. Academic Press, New York, 1982.
8. Jacobs, P. A., *Stud. Surf. Sci. Catal.* **12,** 71 (1982).
9. Gallezot, P., and Bergeret, G., *Stud. Surf. Sci. Catal.* **12,** 167 (1982).
10. Chen, N. Y., and Weisz, P. B., *Chem. Eng. Prog. Symp. Ser.* **63,** 86 (1967).
11. Weisz, P. B., *Pure Appl. Chem.* **52,** 2091 (1980).
12. Rabo, J. A., Schomaker, V., and Pickert, P. E., *in* "Proceedings, 3rd International Congress on Catalysis, Amsterdam, 1964" (W. M. H. Sachtler, G. C. A. Schuit, and P. Zwietering, Eds.) Vol. 2, pp. 1264–1275. North-Holland, Amsterdam, 1965.
13. Chen, N. Y., *Fr.* 1,525,454 (1968) through *Chem. Abstr.* **71,** 42776d (1969).
14. Dessau, R. M., *J. Catal.* **77,** 304 (1982).
15. Dessau, R. M., *J. Catal.* **89,** 520 (1984).
16. Gudkov, S. V., Shpiro, E. S., Romanovskii, B. V., Antoshin, G. V., and Minachev, Kh. M., *Izv. Akad. Nauk SSSR, Ser. Khim.*, 2248 (1980); *Bull. Acad. Sci. USSR, Div. Chem. Sci. (Engl. Transl.)*, 1716 (1981).
17. Diegruber, H., Plath, P. J., Schulz-Ekloff, G., and Mohl, M., *J. Mol. Catal.* **24,** 115 (1984).
18. Tolman, C. A., Nappa, M. J., Herron, N., and Stucky, G. D., *in* "Abstracts, The 1984 International Chemical Congress of the Pacific Basin Societies, Honolulu, 1984," No. 07H12. Amer. Chem. Soc., Washington, D.C., 1984.
19. Mizuno, K., Imamura, S., and Lunsford, J. H., *Inorg. Chem.* **23,** 3510 (1984).
20. Chen, N. Y., and Weisz, P. B., U.S. Patent 3,364,136 (1968).
21. Kuehl, G. H., U.S. Patent 4,299,686 (1981).
22. Jacobs, P. A., Tielen, M., Martens, J., and Beyer, H. K., *J. Mol. Catal.* **27,** 11 (1984).
23. Davis, M. E., and Rossin, J. A., *in* "Abstracts, 9th North American Meeting, Houston, 1985," No. B-6. The Catalysis Society, 1985.
24. Taylor, D., and Hanson, B. E., *in* "Abstracts, 189th National ACS Meeting, Miami Beach, 1985," INOR 19. Amer. Chem. Soc., Washington, D.C., 1985.
25. Tsao, Y.-Y. P., and Wong, S. S., U.S. Patent 4,472,517 (1984).
26. Huang, T.-N., and Schwartz, J., *J. Amer. Chem. Soc.* **104,** 5244 (1982).
27. Nazar, L. F., Ozin, G. A., Hugues, F., Godber, J., and Rancourt, D., *J. Mol. Catal.* **21,** 313 (1983).
28. Ozin, G. A., Nazar, L. F., and Hugues, F., Eur. Pat. Appl. 115,188 (1984) through *Chem. Abstr.* **101,** 137987a (1984).
29. Lewis, P. H., *J. Catal.* **11,** 162 (1968).
30. Wilson, G. R., and Hall, W. K., *J. Catal.* **17,** 190 (1970).
31. Kubo, T., Arai, H., Tominaga, H., and Kunugi, T., *Bull. Chem. Soc. Japan* **45,** 607 (1972).
32. Dalla Betta, R. A., and Boudart, M., *in* "Proceedings, 5th International Congress on Catalysis, Palm Beach, 1972" (J. W. Hightower, Ed.), pp. 1329–1337. North-Holland, Amsterdam, 1973.
33. Czárán, E., Schnabel, K.-H., and Selenina, M., *Z. Anorg. Allg. Chem.* **410,** 225 (1974).
34. Gallezot, P., Alarcon-Diaz, A., Dalmon, J.-A., Renouprez, A. J., and Imelik, B., *J. Catal.* **39,** 334 (1975).
35. Gallezot, P., Mutin, I., Dalmai-Imelik, G., and Imelik, B., *J. Microsc. Spectrosc. Electron.* **1,** 1 (1976).
36. Vedrine, J. C., Dufaux, M., Naccache, C., and Imelik, B., *J. Chem. Soc., Faraday Trans. 1* **74,** 440 (1978).
37. Gallezot, P., Bienenstock, A. I., and Boudart, M., *Nouv. J. Chim.* **22,** 263 (1978).
38. Exner, D., Jaeger, N., and Schulz-Ekloff, G., *Chem.-Ing.-Tech.* **52,** 734 (1980).
39. Lunsford, J. H., and Treybig, D. S., *J. Catal.* **68,** 192 (1981).
40. Reagan, W. J., Chester, A. W., and Kerr, G. T., *J. Catal.* **69,** 89 (1981).
41. Moraweck, B., and Renouprez, A. J., *Surf. Sci.* **106,** 35 (1981).
42. DeMenorval, L.-C., Fraissard, J. P., and Ito, T., *J. Chem. Soc., Faraday Trans. 1* **78,** 403 (1982).
43. Exner, D., Jaeger, N., Möller, K., and Schulz-Ekloff, G., *J. Chem. Soc., Faraday Trans. 1* **78,** 3537 (1982).
44. Chester, A. W., *J. Catal.* **86,** 16 (1984).
45. Friedman, R. M., Gross, D. E., Hershman, A., and Jakse, F. P., *Appl. Catal.* **11,** 147 (1984).
46. Argauer, R. J., and Landolt, G. R., U.S. Patent 3,702,886 (1972).
47. Howden, M. G., "The Role of the Tetrapropylammonium Template in the Synthesis of Zeolite ZSM-5, CSIR Report CENG 413," NTIS Report PB83-247718 (1982).
48. Rollmann, L. D., and Valyocsik, E. W., *Inorg. Synth.* **22,** 67 (1983).
49. Chu, P., and Dwyer, F. G., *ACS Symp. Ser.* **218,** 59 (1983).
50. Olson, D. H., Haag, W. O., and Lago, R. M., *J. Catal.* **61,** 390 (1980).

51. Delk II, F. S., and Vāvere, A., *J. Catal.* **85,** 380 (1984).
52. Jakse, F. P., Friedman, R. M., Delk II, F. S., and Bulock, J. W., *Appl. Catal.* **14,** 303 (1985).
53. Breck, D. W., "Zeolite Molecular Sieves," pp. 93–94, 177. Wiley, New York, 1974.
54. McDaniel, C. V., and Maher, P. K., *in* "Zeolite Chemistry and Catalysis" (J. A. Rabo, Ed.), ACS Monogr. No. 171, pp. 285–331. Amer. Chem. Soc., Washington, D.C., 1976.
55. Smith, D. J., White, D., Baird, T., and Fryer, J. R., *J. Catal.* **81,** 107 (1983).
56. Anderson, D. R., *in* "Analysis of Silicones" (A. L. Smith, Ed.), pp. 247–286. Wiley, New York, 1974.
57. Ribeiro, F. R., *in* "Zeolites: Science and Technology" (F. R. Ribeiro, A. E. Rodrigues, L. D. Rollmann, and C. Naccache, Eds.), pp. 545–569. Nijhoff, The Hague, 1984.
58. Exner, D., Jaeger, N. I., Nowak, R., Schulz-Ekloff, G., and Ryder, P., *Geterog. Katal.* 5th, Pt. 2, 13 (1983).
59. Jaeger, N. I., Ryder, P., and Schulz-Ekloff, G., *Stud. Surf. Sci. Catal.* **18,** 299 (1984).
60. Acosta N., D. R., and Dominguez E., J. M., *in* "Proceedings, 43rd Annual Meeting of the Electron Microscopy Society of America, Louisville, 1985" (G. W. Bailey, Ed.), pp. 374–375. San Francisco Press, San Francisco, 1985.
61. Cody, I. A., U.S. Patent 4,451,572 (1984).
62. Rodewald, P. G., U.S. Patent 4,477,583 (1984).
63. Niwa, M., Kato, S., Hattori, T., and Murakami, Y., *J. Chem. Soc., Faraday Trans. 1* **80,** 3135 (1984).
64. Baldwin, V. H., Jr., and Hudson, J. B., *J. Vac. Sci. Technol.* **8,** 49 (1971).
65. Abbas, N. M., and Madix, R. J., *Appl. Surf. Sci.* **7,** 241 (1981).
66. McCabe, R. W., and McCready, D. F., *Chem. Phys. Lett.* **111,** 89 (1984).
67. Walker, J. F., "Formaldehyde," pp. 52–82. Reinhold, New York, 1964.
68. Heyns, K., and Paulsen, H., *in* "Newer Methods of Preparative Organic Chemistry" (W. Foerst, Ed.), Vol. II, pp. 303–335. Academic Press, New York, 1963.
69. Nandi, R. K., Molinaro, F., Tang, C., Cohen, J. B., Butt, J. B., and Burwell, R. L., Jr., *J. Catal.* **78,** 289 (1982).
70. Olson, D. H., and Haag, W. O., *ACS Symp. Ser.* **248,** 275 (1984).
71. Nunan, J., Cronin, J., and Cunningham, J., *J. Catal.* **87,** 77 (1984).
72. Nayak, V. S., and Choudhary, V. R., *Appl. Catal.* **9,** 251 (1984).
73. Inui, T., Fukuda, K., Morinaga, N., and Takegami, Y., *J. Japan Pet. Inst.* **27,** 188 (1984).
74. Anderson, J. R., Foger, K., Mole, T., Rajadhyaksha, R. A., and Sanders, J. V., *J. Catal.* **58,** 114 (1979).
75. Kikuchi, E., Hatanaka, S., Hamana, R., and Morita, Y., *J. Japan Pet. Inst.* **25,** 69 (1982).
76. Zhou, R., An, S., and Liu, Z., *Cuihua Xuebao* **4,** 303 (1983) through *Chem. Abstr.* **100,** 138328c (1984).
77. Namba, S., Nakanishi, S., and Yashima, T., *J. Catal.* **88,** 505 (1984).
78. Qin, G., Zheng, L., Xie, Y., and Wu, C., *J. Catal.* **95,** 609 (1985).
79. Ramdas, S., Thomas, J. M., Betteridge, P. W., Cheetham, A. K., and Davies, E. K., *Angew. Chem. Int. Ed. Engl.* **23,** 671 (1984).